



Originally published as:

Benduhn, F., Lawrence, M. G. (2013): An investigation of the role of sedimentation for stratospheric solar radiation management. - *Journal of Geophysical Research: Atmospheres*, 118, p. 7905-7921.

DOI: <http://doi.org/10.1002/jgrd.50622>

## An investigation of the role of sedimentation for stratospheric solar radiation management

F. Benduhn<sup>1,2</sup> and M. G. Lawrence<sup>1,2</sup>

Received 20 December 2012; revised 11 May 2013; accepted 29 June 2013; published 26 July 2013.

[1] Gravitational settling has been considered to be one of the limiting factors to stratospheric aerosol lifetime and therefore to the practicability and effectiveness of stratospheric solar radiation management (S-SRM, which is one of the approaches being considered for planetary-scale *geoengineering* or *climate engineering*). Given the property of numerical diffusion that is associated with sedimentation as a transport process on a discretized global grid, it is important to represent this process as accurately as possible. In this paper, newly developed sedimentation schemes are presented and validated against an analytical solution. Sensitivity studies with an aerosol chemistry general circulation model are conducted with monodisperse aerosol particles of fixed size and follow two main aims: first, to evaluate the relevance of sedimentation for the aerosol lifetime and distribution in the stratosphere as a function of particle size, and second, to explore the influence of numerical diffusion on these patterns. The relevance of sedimentation is explored further with respect to other relevant particle properties, such as shape and density. It is shown that the role of sedimentation in determining stratospheric particle lifetime is a complex function of all particle properties combined. Especially with respect to sulfate aerosol, the influence of sedimentation is conditioned by the temporal evolution of particle size. Although large enough particles for considerable sedimentation mediated removal are observed in the context of volcanic eruptions, it seems uncertain whether secondary particles of an equivalent size would be obtained in the context of S-SRM, pointing to the need for an accurate representation of aerosol growth dynamics.

**Citation:** Benduhn, F., and M. G. Lawrence (2013), An investigation of the role of sedimentation for stratospheric solar radiation management, *J. Geophys. Res. Atmos.*, 118, 7905–7921, doi:10.1002/jgrd.50622.

### 1. Introduction

[2] Following an essay by *Crutzen* [2006], there has been an increasing discussion of the use of a man-made aerosol layer in the stratosphere as a potential means to counterbalance the effects of anthropogenic global warming. The purported main prospective advantages of stratospheric solar radiation management (S-SRM) with respect to other options are the technical feasibility of the method, the comparably low costs, the short time scale for development and deployment, its high effectiveness, and a low level of risks [*Vaughan and Lenton*, 2011]. The high effectiveness and controllable level of risks are derived from the supposed analogy of the method with the natural occurrence of large volcanic eruptions (see *Robock et al.* [2013] for a discussion of the limitations of the volcanic analog). A certain number of studies have recently been published that analyze the

prospective side effects of S-SRM. For instance, *Bala et al.* [2008] investigated the effect of a decrease of the global solar radiation on the water cycle, whereas *Tilmes et al.* [2009] assessed the influence of stratospheric geoengineering on global ozone formation and depletion and on polar ozone in relationship with the polar vortex in particular. Recently, the studies of *Heckendorn et al.* [2009], *Pierce et al.* [2010], and *English et al.* [2012] focused on the uncertainties related to subscale and global aerosol particle dynamics with respect to the relationship between the mass of annually injected sulfur and the obtained surface cooling effect. Particle dynamics steer the size distribution spectrum within the modified aerosol layer, which in turn affects its tendency to be removed from the stratosphere by gravitational settling (henceforth simply called sedimentation for simplification). Sedimentation is related to particle size via its dependence on the so-called terminal fall velocity (see below). As such, it could be expected that sedimentation is a major factor contributing to the uncertainty in the lifetime of the modified stratospheric aerosol layer, along with large-scale transport and stratosphere-troposphere exchange. Following this argumentation, *Rasch et al.* [2008a] indicate that sedimentation is the driving process for aerosol removal from the stratosphere, resulting in the observed aerosol lifetime of the order of 1 year following volcanic injections, and could therefore be

<sup>1</sup>Max Planck Institute for Chemistry, Mainz, Germany.

<sup>2</sup>Now at Institute for Advanced Sustainability Studies, Potsdam, Germany.

Corresponding author: F. Benduhn, Institute for Advanced Sustainability Studies, Berliner Strasse 130, Potsdam DE-14467, Germany. (francois.benduhn@mpic.de)

the limiting factor to the cost effectiveness of S-SRM techniques in terms of aerosol mass injection requirements.

[3] This paper attempts to provide further insight into the role that sedimentation plays in limiting the effectiveness of S-SRM. In order to examine this, the characteristics of particle sedimentation with respect to S-SRM need to be considered. Here we divide these characteristics into two categories. First of all, the study of sedimentation in the framework of S-SRM requires the consideration of both microphysical and global transport-related elements that take place on diverse scales of time and space. The problems associated with this characteristic are related to those treated by *Pierce et al.* [2010] for aerosol growth dynamics. Second, the evaluation of the role sedimentation plays for stratospheric particle lifetime may suffer from inherent weaknesses linked to its representation within global models that operate on discretized grids and may also be limited by computational efficiency considerations. Within this paper, we focus mainly on the second point. Doing so, we will assess whether sedimentation may in principle serve as a limiting factor for the lifetime of the modified aerosol layer and, in the affirmative case, identify the properties of the limiting process. The set of problems that derives from the first category, in particular, the interaction of particle growth dynamics, sedimentation, and global circulation, will be treated in greater detail in a follow-on publication.

## 2. Issue and Method

[4] Let us examine now the general properties of particle sedimentation in the atmosphere, the issues related to its representation within a global modeling environment, and its relationship to the particular characteristics of sedimentation within a stratosphere subjected to S-SRM.

[5] Aerosol particle movement in the atmosphere through sedimentation is the result of the competing forces of gravitation and friction exerted by the air medium. As such, it is particle size and mass dependent and therefore takes places relative to the air medium. In atmospheric modeling, it is generally represented as the balance between the two driving forces, the formulation of which is relatively straightforward [*Pruppacher and Klett, 1997; Jacobson, 1999*]. The resulting equilibrium fall velocity, the so-called terminal velocity of an aerosol particle of a particular size and mass, additionally depends on the air dynamic viscosity and density, which may be expressed or estimated as a function of height. For this reason, the gravitationally induced movement of an aerosol particle relative to the air could be computed on a discretized time axis with a relatively high accuracy, were it not for the concurrent vertical discretization of the Eulerian grid, which inherently leads to numerical diffusion. As a matter of fact, any continuous process that is treated on a discretized Eulerian domain is subject to numerical diffusion. Both the so-called downwind representation of sedimentation and the nodal representation of aerosol growth through condensation and coagulation are inherently diffusive. Several attempts have been made to reduce numerical diffusion in the general context of atmospheric transport, and advection, which is the most relevant conceptual transport process within atmospheric modeling, has been given particular attention. Thus, low-diffusion solutions to advection might also serve

as accurate solutions to atmospheric sedimentation of aerosol particles, in as much as these two processes are formally compatible.

[6] The relevance of sedimentation to aerosol transport and mean lifetime is manifold. As a standalone process, sedimentation is driven by the aerosol particles' terminal velocity. However, relative to competitive transport and removal processes, the importance of sedimentation depends on their occurrence and magnitude. For tropospheric aerosol, sedimentation is typically an effective transport process for coarse-mode aerosol particles, for which it may compete effectively with cloud- and precipitation-related wet removal processes and with advective transport via the large-scale flow of the atmosphere. For submicrometer particles, the tropospheric mean aerosol lifetime of about 7 days [*Hobbs, 1993*] is too short for sedimentation, with typical terminal velocities of less than  $10^{-5} \text{ m s}^{-1}$  [*Seinfeld and Pandis, 1998*], to compete with wet removal processes. However, for stratospheric aerosol particles, the picture is quite different. On the one hand, the terminal velocity of aerosol particles of a given size increases substantially with height due to its dependence on the Cunningham slip flow correction factor [see, e.g., *Pruppacher and Klett, 1997*]. The mean free path increases with height as the air molecule number density decreases and so do both the Cunningham factor and the terminal velocity. Thus, the terminal velocity of 100 nm particles is about  $3 \mu\text{m s}^{-1}$  at sea level, while its corresponding velocity at 25 km is equivalent to ca.  $5 \text{ mm s}^{-1}$ . On the other hand, competitive transport processes such as the vertical component of advection, convection, small-scale turbulent mixing, and wet removal are generally either relatively slow or nonexistent above the tropopause.

[7] Thus, sedimentation is likely to be a decisive process for aerosol lifetime in the stratosphere in general, as well as for the feasibility and effectiveness of S-SRM in particular, while a limiting factor to its accurate representation within global models may be linked to the numerical diffusion property of the scheme that is being used. In consideration of this, we will explore pathways to reduce numerical diffusion of sedimentation via the development of specific numerical integration methods on a spatially discretized grid. In particular, methods developed for the special representation of advection as an atmospheric transport process will be considered and, if found suitable, adapted to the special purpose of sedimentation. The new methods will be validated against an analytical solution for an idealized atmosphere and compared to preexisting schemes, in particular, with respect to their reduced numerical diffusion properties. After their implementation into the global chemistry aerosol general circulation model EMAC (ECHAM5 Model of Aerosols and Atmospheric Chemistry [*Joeckel et al., 2006*]), their capacity to represent this process more accurately in terms of the reduction of numerical diffusion will be evaluated in the framework of a stratosphere subjected to S-SRM. To this purpose, a sensitivity study that uses monodisperse aerosol particles of given fixed size is carried out. The choice of micrometer-sized particles for this sensitivity study is justified with a theoretical aerosol microphysical argumentation. It is argued that the simulated global aerosol burden as a function of particle size may be related to the particle terminal velocity at a certain characteristic height. Following this procedure, a conceptual generalization of the

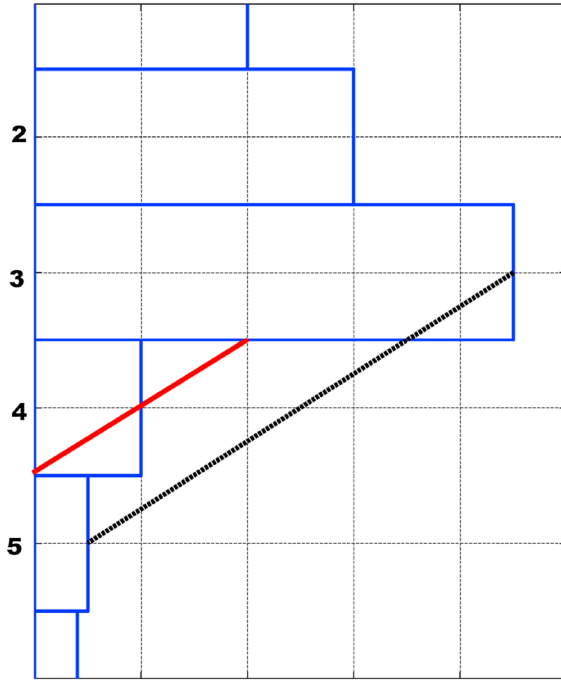


**Figure 1.** Numerical principle of the *Walcek* [2000] advection scheme. The vertically discretized tracer concentration as a function of height is indicated by the blue bars, each one standing for one grid box. The local gradient in grid box 4 is given by its neighbors 3 and 5, and translated so that it goes through the center of the grid box.

particle sedimentation loss rate as a function of size is obtained, which will provide an insight into the relevance of sedimentation as a function of other particle properties that determine their terminal velocity, such as density and shape. An indication about the relevance of sedimentation to the lifetime of S-SRM aerosol particles as a function of their combined sedimentation-relevant properties will thereby be obtained.

### 3. Theory

[8] On a vertically discretized dimension  $z$ , the amount of sedimenting particles lost from a particular grid box per unit surface area within one time step  $\Delta t$  is

$$\Delta N = \int_{\Delta t} n v dt,$$

where  $n$  is the number of particles per unit volume and  $v$  is the terminal velocity of the particles, both being time-dependent values at the model layer interface.

[9] A considerable formal simplification is attained if the terminal velocity is considered to be constant throughout the grid cell and over the time step:

$$\Delta N = \int_{\Delta z=v\Delta t} n dz.$$

[10] The maximum possible simplification is achieved by the upstream model, which assumes that  $n$  is constant as well within the grid cell, so that  $\Delta N = n\Delta z$ . However, this assumption induces a high degree of numerical diffusion, since the aerosol particles that are transported to the underlying grid

cell directly become available for transport into the next layer down already during the next time step. As a consequence, the distance a sedimenting aerosol particle may cover within a certain amount of time on a discretized grid is not only a function of the sedimentation velocity but also depends arbitrarily on the chosen time increment and vertical resolution of the grid, with the distance that can potentially be covered becoming larger for lower spatial and higher temporal resolutions.

[11] If the vertical distributions of both  $n$  and  $v$  were to be known continuously as a function of time, then it would be theoretically possible to determine a highly accurate solution for the sedimentation with virtually no numerical diffusion. A step down from this are so-called higher-order methods, which try to mimic this optimal situation by carrying information on the subgrid-scale distribution of the parameters within the grid cells, e.g., by carrying the subgrid-scale vertical gradients as moments, up to a certain prechosen degree [e.g., *Prather*, 1986]. However, the application of such schemes quickly becomes technically complex in atmospheric models, which simulate concurrent transport processes that are integrated separately in time (operator splitting). In such cases, the application of a higher-order method for sedimentation is nontrivial, as it would require both the exchange of additional information between the sedimentation and advection schemes, and the preservation of this subgrid-scale information through all other process modules (e.g., aerosol microphysics); this also increases the computational expense considerably. Thus, we have chosen not to consider such higher-order methods in this study.

[12] Another approach to reduce numerical diffusion is to guess the approximate subgrid-scale distribution of the transported tracer, usually by considering the relationship between its concentration in the grid cell in question and its (average) concentration in the neighboring grid cells. This is the underlying principle of the “trapezoidal” method for sedimentation, which was implemented in EMAC by *Kerkweg et al.* [2006], as well as of the advection scheme by *Walcek* [2000]. Due to the uncertainty that is related to the repetitive reconstruction of the subgrid-scale distribution after each time increment, these methods may show a greater tendency for numerical diffusion and/or inaccuracy than higher-order methods. Thus, the trapezoidal method follows an ad hoc principle in as much as it is aimed at conserving extrema in the vertical distribution via a utilitarian but arbitrary choice that is operated on the representative internal gradient [*Kerkweg et al.*, 2006]. On the other hand, the principle of the *Walcek* scheme, as depicted in Figure 1 for the case of a sedimenting quantity, invariably considers both the adjacent upstream and the downstream grid boxes to obtain a first guess on the internal distribution within a certain grid box. The conceptual aspect of its first guess shows up in inconsistencies that appear in the spatial distribution of the transported variable, such that advected quantities may develop artifacts under the shape of new absolute extrema in terms of mixing ratio. *Walcek* [2000] therefore integrated a monotonicity fixer into his advection scheme, which efficiently acts as a correction to the first-guess gradient so that nonphysical evolution scenarios of the transported variable are avoided.

[13] At this point, it needs to be clarified whether the *Walcek* advection scheme may be applied ad hoc to other

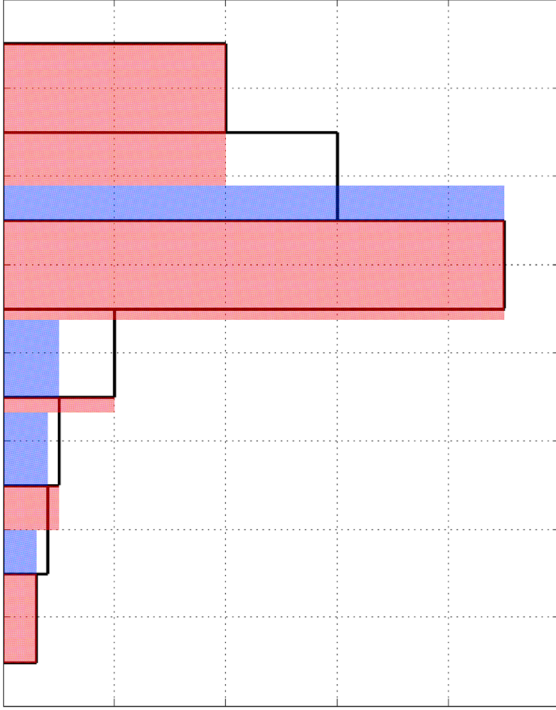


**Figure 2.** Numerical principle of the pseudo-equilibrium scheme on a vertically discretized grid. Each grid box (in black) is split in two parts (upstream: in red; downstream: in blue). The value associated with these parts is given by their respective neighbor; their width is such that their total content is equivalent to the actual content.

transport processes, among them sedimentation, which is in effect tantamount to the question if advection and sedimentation are formally similar processes. While advection is a mixing ratio conserving (i.e., “monotonic”) process, aerosol sedimentation is not, as particles essentially move independently from the air molecules. In addition, particle velocity is not a constant over the discretized domain, because both air density and particle size and composition vary with height. As a consequence, aerosol sedimentation may produce new absolute extrema, and the monotonicity fixer within the Walcek scheme may not be applied. If the Walcek scheme is to be used for sedimentation as an alternative transport process, a different formalism needs to be developed to define and eliminate inappropriate gradients resulting in unrealistic flows.

[14] To do this, we will start by considering which information we actually have within first-order transport schemes. Initially the transported entity has to be considered to be homogeneously distributed within the individual grid cells, as this is the inherent underlying assumption of zeroth-order discretized domain decomposition. In the absence of any concurrent transport process, the particle distribution within a certain grid box  $i$  would therefore be after  $a$  time steps  $\Delta t$ :

$$\bar{n}_i|_{a\Delta t} = \zeta_{i-1}n_{i-1}|_{t=0} + \zeta_i n_i|_{t=0},$$

where  $\zeta_{i-1}$  is the fraction of aerosol within grid box  $i$  that emanates from the upstream grid box  $i-1$  and  $\zeta_i$  is the remaining fraction of the original aerosol from grid box  $i$ . The equation  $\zeta_{i-1} = 1 - \zeta_i$  would hold as long as the aerosol has not moved through the entire grid box.

[15] In the absence of a concurrent transport process, it would therefore be sufficient to monitor how far the aerosol from the upstream grid box has moved into the considered grid box and what fraction of the considered grid has been emptied within the same time interval to know the aerosol content within that grid box. If additionally we assume sedimentation to be monotonic in the individual grid box, we actually end up with two separated blocks of aerosol, one originating from above and the other one being the remaining fraction of the original aerosol. Still, concurrent aerosol transport processes, such as advection, will continuously smear out these two aerosol blocks. As a consequence, all variables on the right-hand side of the above equation will become unknowns and it becomes useless on its own. However, we could guess the properties of the two aerosol blocks with the following simple assumption, which is congenial to the approach used in other schemes of applying certain assumptions to guess the grid box internal distribution:

$$\begin{aligned} \bar{n}_i|_t &= \zeta_{i-1}\bar{n}_{i-1}|_t + \zeta_{i+1}\bar{n}_{i+1}|_t \\ \zeta_{i+1} &= 1 - \zeta_{i-1} \end{aligned}$$

[16] All variables on the right-hand side are known, as for each time step, the fractions  $\zeta$  are solved such that the average concentration in grid box  $i$  is obtained as function of its neighbors  $i-1$  and  $i+1$ . If this decomposition is made for every grid box of the domain except for the extrema, for which the upwind method may be used, and for the limiting grid boxes of the domain, then a picture similar to Figure 2 may be obtained.

[17] This method possesses an implicit property in space because the amount of aerosol transported within one time step from grid box  $i$  to grid box  $i+1$  always depends on grid box  $i+1$ , as the contiguous concentration within grid box  $i$  is supposed to be equal to the one within  $i+1$ . The aerosol flux may also depend explicitly on grid box  $i-1$ , depending on the vertical gradient within the grid box  $i$ , as given by the variables  $\zeta_{i-1}$  and  $\zeta_{i+1}$ , and the distance covered by the aerosol during one time step. The method is thus related to the staggered grid methods, as aerosol and air properties are associated to those at the center of the grid box, while  $n$  is essentially determined at the interfaces. Physically, the method assumes that the system is in pseudo-equilibrium at the level of the individual interface. This assumption actually ensures that no numerical diffusion occurs when transport from  $i$  to  $i+1$  is slow enough to exclusively depend on grid box  $i+1$ . It is noteworthy that under this circumstance, numerical diffusion is not induced by an extremum in  $i$ , as transport from  $i+1$  to  $i+2$  still depends on  $i+2$  only. On the other hand, if transport from  $i$  to  $i+1$  is quick enough to additionally depend on  $i-1$ , numerical diffusion is effectively buffered as it still depends on grid box  $i+1$  as well. In addition, matter thus transported to  $i+1$  at time step  $t$  will influence transport to  $i+2$  at  $t+1$  in an implicit manner only, via the upper fraction  $\zeta_{i-1}$  in grid box  $i+1$ . This circumstance reflects that when transport is quick, matter transported from  $i$  to  $i+1$  at time step  $t$  has to become available for transport to  $i+2$  at time step  $t+1$  unless overall transport is too slow. These considerations will be addressed with further detail in the following section.

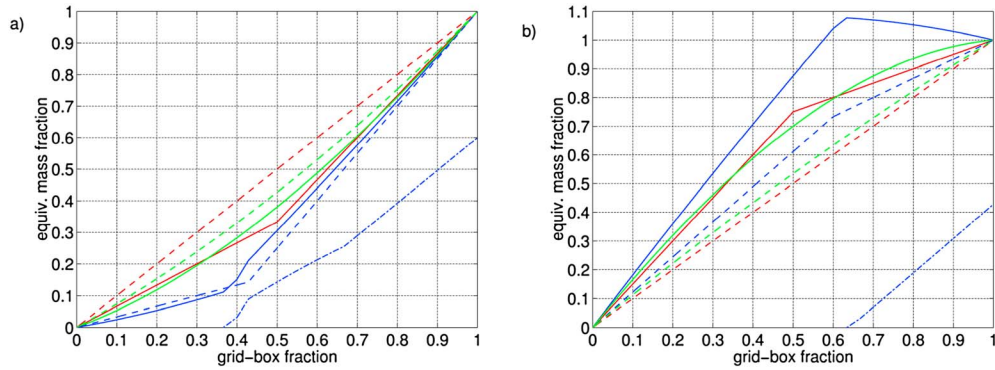


**Figure 3.** Mass flux going into the observed grid box (see text), given as grid box mass fraction, as a function of the grid box volume fraction that is transported during one time step. Results are shown for (a) a negative mass gradient (decreasing mass density into flow direction) and (b) a positive mass gradient, for the Walcek scheme (green), the pseudo-equilibrium scheme (blue), and the benchmark analytical solution transposed to the Eulerian grid (red), respectively. The results shown cover the initial first two time steps. Mass fractions are normalized with the initial content of grid box  $i-2$  (solid lines) and of grid box  $i-1$  (dashed lines), at  $t=2$  and  $t=1$ , respectively. The variable  $\zeta_{i+1}$  (pseudo-equilibrium scheme, see definition in text) of grid box  $i-1$  at  $t=2$  is also shown as given by  $(x-\zeta_{i+1})$ ,  $x$  being the volume fraction of the grid box that is moved (dash-dotted blue line). The salient nonlinearities of the pseudo-equilibrium solution at  $t=2$  are triggered by this variable being larger than zero. For instance, within Figure 3b, the nonlinearity is caused by  $\zeta_{i+1} \approx 0.62$ . Additional minor nonlinearities are apparent and may be related to other  $\zeta$  variables at both  $t=1$  and  $t=2$ .

[18] Now that we have developed an alternative low-numerical diffusion formalism to aerosol transport via sedimentation on a discretized grid, we can explore how it may be combined with the Walcek advection scheme so that the latter may be adapted to the special purpose of sedimentation. As related above, the new scheme shows a certain degree of analogy with the Walcek scheme as it assesses the sedimentation flux from one particular grid box as a function of the contiguous grid boxes. On the other hand, the physical inconsistency related to the Walcek scheme without the monotonicity fixer may for instance result in a misrepresentation of transport when the guessed grid box internal gradient is particularly steep, thus resulting in a nonphysical distortion of transport fluxes, which may eventually result in the formation of new local extrema. Due to its pseudo-equilibrium approach, the new method actually provides a physically consistent minimum value of the sedimentation flux both in the presence of negative and positive gradients. When dealing with a maximum, it may thus serve to provide a lower limit for the sedimentation flux below the maximum, which effectively prevents the formation of new artificial minima, and provide a minimum for the sedimentation flux above a local maximum, so that the existing extremum is effectively preserved, for instance during the settling of an aerosol plume. The slow smearing out of the upper limit of a plume actually corresponds to upward numerical diffusion, which is thus avoided while the lower boundary always settles at a physical minimum speed. The combined Walcek/pseudo-equilibrium thus reads

$$\Delta N_{\text{combined}} = \max(\Delta N_{\text{Walcek}}, \Delta N_{\text{pseudo-equilibrium}}).$$

[19] The appropriateness of this partially conceptual approach is put to the test in the following section.

#### 4. Validation

[20] We will first examine the numerical properties of how the original Walcek scheme and the pseudo-equilibrium scheme behave at the individual grid box level. For this purpose, it may be useful to compare these Eulerian schemes against an analytical solution. The Eulerian schemes will potentially start generating numerical diffusion at the second time step, whereas the analytical approach provides an exact solution of transport that serves as a benchmark. In our example, the setup is such that particles fall at constant speed through a vertical domain consisting of six equally sized grid boxes initially containing a (unitless) particle density of 12, 11, 9, 6, 2, and 0, from top to bottom ( $i=1$  to 6, respectively; see also Figure 1 for an illustration). The time step and sedimentation velocity are chosen such that particles move no farther than one grid box during one time interval. For this reason, the benchmark amount of particles in grid box  $i$  exclusively depends on grid boxes  $i$  and  $i-1$  after one time step. After the second time step, the amount of particles within  $i$  may depend either on the initial amount within  $i$  and  $i-1$ , or on initial  $i-1$  and  $i-2$  depending on the fraction of the grid boxes that is moved during one time step. Experimental results for the mass fraction of grid boxes  $i-2$  and  $i-1$  going into  $i=5$  are shown in Figure 3a as a function of the time step, which is given as the sedimented grid box volume fraction equivalent at  $t=2$  and  $t=1$ , respectively, and increased continuously from zero to the entire grid box moved within one time step. The aerosol mass fractions that are moved are in general dissimilar to the grid box volume fractions, for both the Walcek and the pseudo-equilibrium schemes, since they make assumptions about the internal distribution of the sedimenting aerosol. During the first time step, the pseudo-equilibrium scheme, and to a lesser extent the Walcek scheme, persistently underestimates transport,

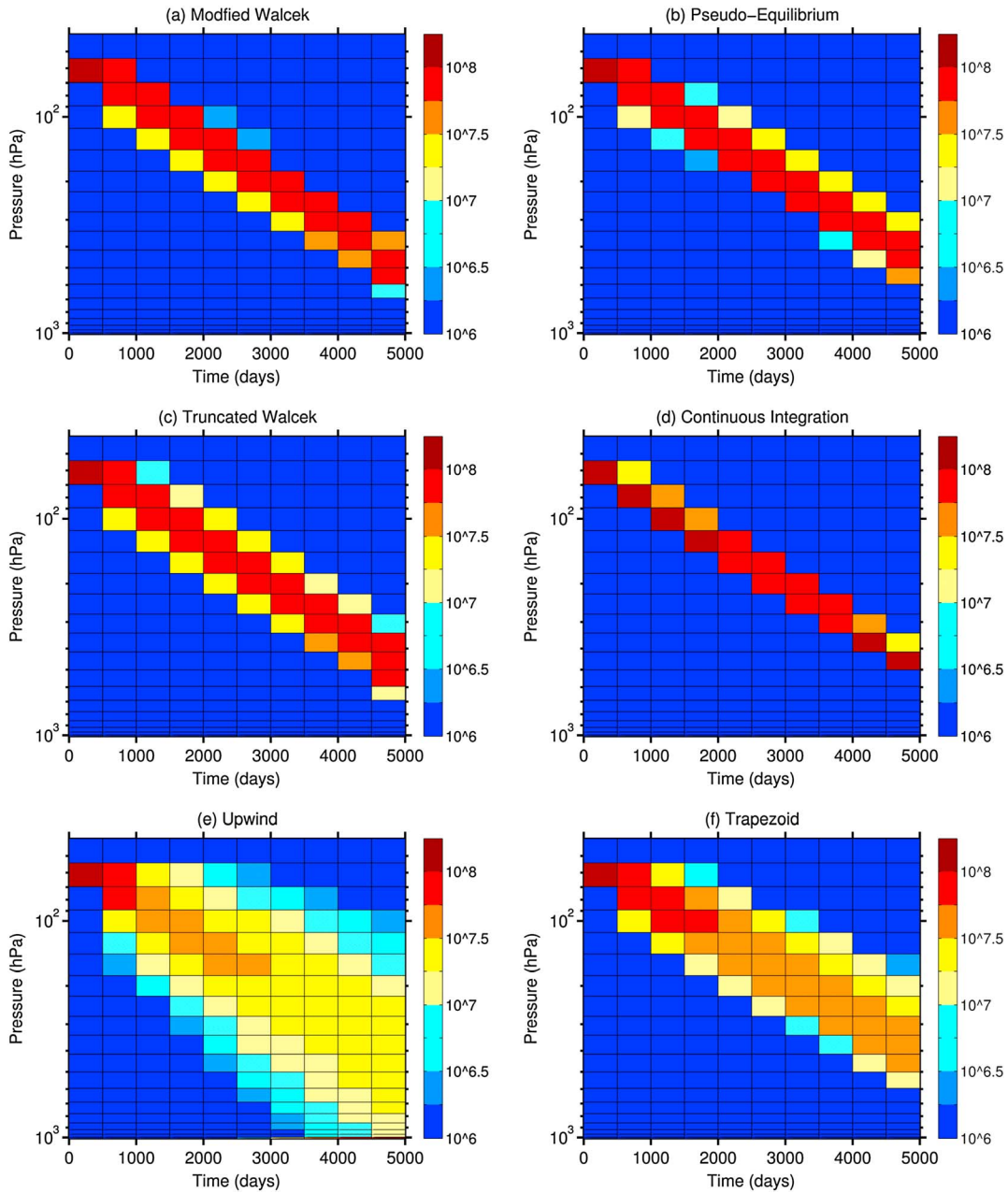


**Figure 4.** Validation of (a) the modified Walcek and (b) the pseudo-equilibrium scheme against the original Walcek scheme without (c) the monotonicity fixer and (d) an analytical solution, and comparison against (e) the upwind scheme and (f) the trapezoid scheme. The tracer content, given as the particle number concentration in standard pressure equivalents ( $\#/m^3$ ) is plotted against the pressure and the time axes. Particles are injected at an initial concentration of  $1.5 \cdot 10^8 m^{-3}$ . The analytical solution is continuously computed using the ideal gas law and the hydrostatic pressure equation to assess the distance in pressure coordinates. Note that the numerical diffusion associated with the upwind scheme eventually induces a large fraction of the total tracer to be located at the lower end of the vertical domain.

as both schemes depend on grid box  $i$  for their flux assessment and the mass gradient is negative (decrease of tracer concentration in flow direction, note the flux from  $i - 1$  into  $i$  is observed at this point). The amount of matter transported by both the Walcek scheme and the pseudo-equilibrium scheme goes through a phase of increasing underestimation, which is then continuously reduced as the fraction of matter transport gets more and more influenced by grid box  $i - 2$ . However, the underestimation of transport is much more

pronounced for the pseudo-equilibrium scheme, as it is exclusively driven by grid box  $i$  in the first place and the onset of the influence of grid box  $i - 2$  marks a discontinuity. For this reason, the Walcek scheme is much closer to the real transport flux during the following time step, and consistently, the transport flux assessed with the pseudo-equilibrium scheme remains well below the actual one when the fraction of the grid box that is moved is relatively low; i.e., it appears to provide a lower bound for the transport. In addition, the fraction

transported by the pseudo-equilibrium scheme becomes more discontinuous from time step  $t = 1$  to  $t = 2$  as the total number of grid boxes, and therefore also local variables  $\zeta$  it depends on, increases from 2 to 6 (see also figure caption). It becomes thereby apparent that in the presence of a negative concentration gradient, the pseudo-equilibrium scheme limits numerical diffusion at the expense of an effective transport velocity that is too low. On the other hand, the Walcek scheme shows a more accurate effective transport velocity, whereas numerical diffusion should be more pronounced. As a corollary, the pseudo-equilibrium scheme should overestimate the transport velocity for a positive tracer concentration gradient, while diffusion will still be reduced. This is confirmed by Figure 3b, which is the counterpart to Figure 3a for a negative gradient (particles are actually now transported in the other direction, namely from  $i = 6$  to  $i = 1$ , and the transport flux from grid box  $i = 3$  into  $i = 2$  is monitored). While the transport velocity of the pseudo-equilibrium scheme is too high, the Walcek scheme produces an effective transport velocity that is comparable to the one obtained with the analytical solution, like previously obtained with a negative mass gradient. The tendency of the pseudo-equilibrium scheme to underestimate transport below a maximum while it overestimates transport above one involves a propensity to “squeeze together” peaks in particle distributions while numerical diffusion is blocked. For this reason, the pseudo-equilibrium scheme is an anti rather than a nondiffusive scheme, and it should be ideal to simulate the transport of pronounced narrow maxima.

[21] The pseudo-equilibrium and the combined pseudo-equilibrium/Walcek scheme (henceforth called *modified Walcek* scheme) may now be compared against an analytical solution of particle sedimentation, given simplified atmospheric conditions. For this purpose, a monolayer of monodisperse aerosol is injected instantaneously at a height of 25 km. All other grid cells are initially set to zero concentration. Particles then immediately begin to settle at a constant terminal velocity throughout the atmosphere (irrespective of its density, to keep the analytical solution simple). The assumed velocity is  $v = 3.5 \cdot 10^{-5} \text{ m s}^{-1}$ , which is representative for particles of  $r = 0.5 \mu\text{m}$  falling under standard temperature and pressure conditions. Also for simplicity, the correspondence between height and pressure is evaluated according to the ideal gas law and hydrostatic conditions assuming an isothermal atmosphere at 250 K. The simulation is run for 5000 days, with no other processes influencing the particles, which is sufficient for them to settle through a large portion of the hypothetical atmosphere. The new numerical schemes are checked against two analytical integrations, one resulting from a continuous integration along the trajectory of the falling particles and a second one resulting from a stepwise integration, which accounts for the discretized nature of the domain in terms of atmospheric pressure. Figure 4 shows the corresponding results. Only the continuous analytical integration results are shown (Figure 4d), as the stepwise integration looks indistinguishable. Both the Walcek (Figure 4a) and the pseudo-equilibrium method (Figure 4b) show a very limited degree of numerical diffusion as the initial monolayer is distributed among four layers at the end of the experiment. Numerical dispersion requires the monolayer to extend over a minimum of two layers. Given the definition of the fraction coefficients,  $\zeta$ , the moderate speed of  $0.5 \mu\text{m}$  particles ensures that the transported aerosol quantity only depends on grid

box  $i - 1$  when its content is approximately equal to the one of grid box  $i$ . Under this circumstance, numerical diffusion cannot be suppressed and the plume may spread into an additional grid box. Mostly, however, the pseudo-equilibrium method effectively blocks any further numerically diffusive transport into downwind grid boxes containing no aerosol. Although the modified Walcek scheme relies on the pseudo-equilibrium approach only for those cases for which the original Walcek scheme would predict an unrealistically low transport flux in the presence of steep gradients, the amount of numerical diffusion it presents is almost as limited as the pseudo-equilibrium scheme. The numerical role of the pseudo-equilibrium scheme within the modified Walcek scheme is illustrated by Figure 4c, which shows results obtained with the (truncated) Walcek scheme without the original monotonicity fixer. Without the inherent numerical diffusion suppressing property of the pseudo-equilibrium scheme, the Walcek scheme shows a higher propensity to smearing out local extrema. On the other hand, the slightly slower effective settling velocity given by the pseudo-equilibrium scheme is not obtained with the modified Walcek scheme, as within this scheme the former only serves to provide a realistic minimum value. The correct representation of the effective settling velocity within the modified Walcek scheme is demonstrated when it is compared to the analytical solution (Figure 4d). It appears that both the pseudo-equilibrium and the modified Walcek scheme capture the settling velocity fairly well on the discretized domain, although the new scheme effectively turns out to be slightly too slow, as anticipated above. The relevance of effective numerical diffusion reduction for the assessment of the effective transport velocity is demonstrated when the new schemes are compared against the frequently used upwind scheme (Figure 4e) and the *Kerkweg et al.* [2006] trapezoid scheme (Figure 4f). The numerical diffusion caused by the upwind scheme is so significant that a large fraction of particles—more than 30%—has reached ground by the end of the experiment, as the initial peak has been smeared out through the entire underlying domain. Although showing a reduced amount of numerical diffusion when compared to the upwind scheme, the trapezoid scheme still shows a substantially higher amount than the modified Walcek and the pseudo-equilibrium scheme. Also, the settling velocity of the particles is somewhat underestimated with the trapezoid scheme.

## 5. Three-Dimensional Experimental Setup

[22] The pseudo-equilibrium scheme and the modified Walcek scheme have been implemented within the EMAC global chemistry–general circulation model [Joeckel et al., 2006]. We use passive tracers of fixed particle size injected into the stratosphere above the equator at an equivalent height of 25 km at a rate of 10 Mt S per annum. The model is run at the T42L39MA resolution (equivalent to an approximately  $2.8125 \times 2.8125^\circ$  horizontal grid spacing, 39 vertical levels from the ground to the top of the atmosphere) for 4 years from 2001 to 2004. Passive tracers are ideal for the exploration of the relevance of sedimentation for the lifetime of S-SRM aerosol particles, since the absence of microphysical processes (nucleation, condensation, evaporation, and coagulation) ensures constant aerosol radius and therefore continuous influence of sedimentation on the particles. The

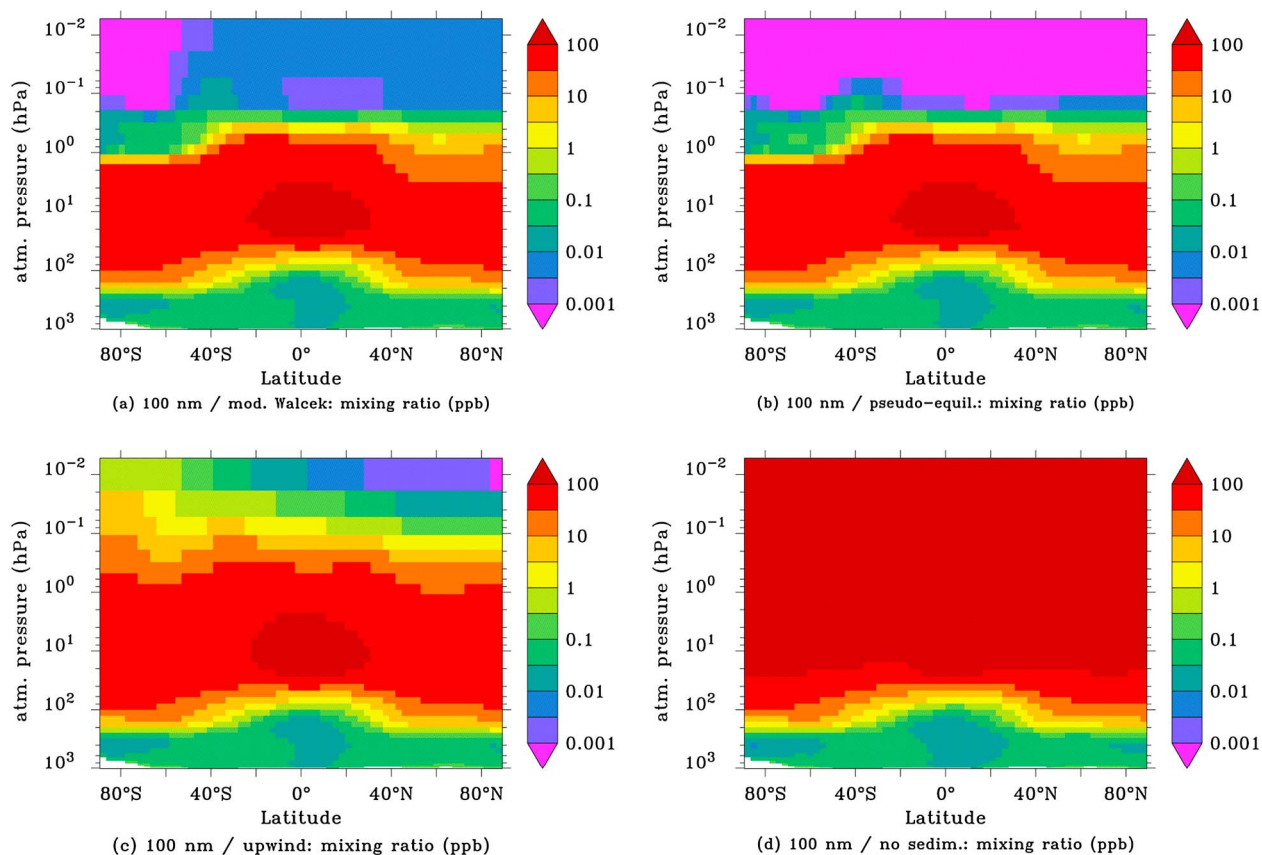


**Figure 5.** Zonal mean plot of the sulfur molecule mixing ratio equivalent of 100 nm particles obtained with (a) the modified Walcek scheme, (b) the pseudo-equilibrium scheme, (c) the upwind scheme, and (d) when sedimentation is switched off. Values shown are averaged for December 2004 after a period of 4 years of circum-equatorial injection at 10 Mt/a of sulfur.

aerosol is allowed to be scavenged from the atmosphere through wet removal processes, as well as to deposit onto the Earth's surface, to prevent the buildup of unrealistic particle distributions in the troposphere. The particles are assumed to be composed of a highly concentrated binary sulfuric acid water mixture. With passive tracers of fixed size, the exact composition is relevant only for particle density, which influences their terminal velocity. For this reason the assumption of  $\text{H}_2\text{SO}_4\text{-H}_2\text{O}$  may be a good approximation for stratospheric conditions within this study.

[23] Four series of experiments have been carried out in order to explore the sensitivity of sedimentation to particle size. The first series is done with particles of 100 nm radius. Particles of about 100 nm size have been estimated to have optimal properties for S-SRM [e.g., *Rasch et al.*, 2008b], owing to the relationship between the aerosol size, the required mass injection rate, and its shortwave radiation reflection properties. Submicrometer particles present the advantage of not significantly absorbing infrared radiation [*Lacis et al.*, 1992] but have the disadvantage of enhanced heterogeneous reactivity due to their higher surface to volume ratio at constant total aerosol mass, which may enhance ozone depletion [e.g., *Tilmes et al.*, 2009]. The second series of experiments is carried out with 500 nm particles. Particles of this size are supposed to represent a typical size that may be obtained through microphysical growth processes and the elongated time intervals that typically go with secondary

particle residence in the stratosphere. It is therefore interesting to assess whether significantly increased losses through sedimentation may occur at this size, when compared to 100 nm particles. The third series of experiments considers 1  $\mu\text{m}$  particles. This size was chosen (1) as an upper limit size beyond which infrared absorption increases significantly, (2) as an estimated threshold size beyond which sedimentation losses should be substantial, and (3) as a speculative maximum size that may be reached via microphysical growth processes in the context of S-SRM. The fourth series concerns 5  $\mu\text{m}$  particles. Although this is a size not usually associated with secondary particles, stratospheric particles of this size do occur in the framework of volcanic eruptions [e.g., *Russell et al.*, 1996; *Stenchikov et al.*, 1998]. As volcanic eruptions are frequent occurrences, which in addition are frequently compared to S-SRM (see above), such that the results of the present study may be of interest for a reader with a background in either volcanic eruptions or S-SRM, or both, we extended the explored parameter space to particle sizes typical for stratospheric volcanic aerosol.

[24] Whether micrometer-sized secondary particles may really form in substantial amounts in the context of S-SRM via coagulation and condensation should deserve a more detailed exploration. The details of this exploration are given in Appendix A, and we will only summarize here the main findings. On longer time scales, the growth of secondary particles may be associated exclusively with coagulation, as

**Table 1.** Aerosol Global Burden and Lifetime

	Burden <sup>a</sup> (%)	Lifetime <sup>b</sup> (years)
No sedimentation	30.016 Mt S	3.0016
100 nm		
Modified Walcek	93.18%	2.7968
Pseudo-equilibrium	93.39%	2.8032
Upwind	93.50%	2.8064
500 nm	0.00%	
Modified Walcek	67.59%	2.0288
Pseudo-equilibrium	68.98%	2.0704
Upwind	68.44%	2.0544
1000 nm	0.00%	
Modified Walcek	40.38%	1.2122
Pseudo-equilibrium	41.95%	1.2592
Upwind	42.43%	1.2736
5000 nm	0.00%	
Modified Walcek	4.29%	0.1286
Pseudo-equilibrium	4.22%	0.1267
Upwind	4.48%	0.1344

<sup>a</sup>Given as percentage of the global burden16 without sedimentation, at the end of the experiment.

<sup>b</sup>Given as  $e$ -folding time of the total removal rate (see text).

sulfuric acid may be assumed to condense rapidly onto freshly nucleated particles after its release into the atmosphere [Turco and Yu, 1997]. Furthermore, owing to the long time intervals involved, the resulting aerosol size spectrum should be self-preserving [Friedlander and Wang, 1966], the growth characteristics of which may be related to a monodisperse aerosol. The relationship between the time interval of formation ( $\Delta t$ ), the relevant coagulation kernel ( $k$ ), and aerosol number concentration ( $n$ ) may then be given by the following:

$$\Delta t \approx \langle k \rangle^{-1} n^{-1}.$$

[25] The preceding equation implies that (paradoxically) the growth interval does not depend explicitly on particle size. The relationship between particle number concentration and particle size can be established with the mass conservation equation, given an estimation of the depth of the stratospheric aerosol layer. One may then derive that particles should on average take between 3 and 30 years to reach micrometer size, whereas after 1 year, the mass fraction concentrated in particles larger than 1  $\mu\text{m}$  in radius should be between 0.05 and 0.175. With these findings, the formation of micrometer-sized particles may not be excluded from a growth dynamical point of view, although a massive formation seems to be unlikely. For this reason, their inclusion in a sensitivity study on the sedimentation of aerosol particles from a stratosphere perturbed by S-SRM makes sense, although the results may only be of relevance for a relatively small component of the overall aerosol distribution.

## 6. Results

[26] Figures 5a–5d show zonal mean plots of the monodisperse 100 nm aerosol distribution averaged for December 2004 for the modified Walcek, the pseudo-equilibrium, and the upwind schemes, as well as with sedimentation switched off, respectively. It appears that sedimentation effectively limits upward transport of the aerosol within the stratosphere, as switching off sedimentation results in the tracer being

distributed nearly homogeneously above the tropopause. Obviously, such a picture could not be obtained in the presence of evaporation, which in effect precludes transport of sulfate aerosol particles to the upper stratosphere. In the troposphere, the picture is comparable for all runs, which is because sedimentation is a relevant transport process for 100 nm particles within the stratosphere, while once in the troposphere particle, distribution is dominated by transport with the air flow and removal processes. When compared to the upwind scheme, both the modified Walcek and the pseudo-equilibrium schemes are much more effective in limiting upward transport than the upwind scheme and produce a much sharper separation between the S-SRM aerosol layers and those above, which underlines the low-diffusion property of these schemes.

[27] It is somewhat paradoxical that the limitation of numerical diffusion affects mainly those layers that are situated in the opposite direction of the sedimentation flow. This feature is a result of the competition between sedimentation and the ascending airflow in the Brewer-Dobson circulation. A low-diffusive sedimentation scheme will diagnose this flow as a high vertical gradient of the aerosol within affected grid boxes and will thereby sediment particles back effectively toward the underlying grid box (i.e., within one time step, the particles will be transported upward by the advection but then back downward in a relatively shape-preserving manner by the low-diffusive sedimentation schemes). However, the numerical diffusion in the upwind scheme smears the aerosol layer out in both directions (up and down), and the aerosol that is smeared out in the upward direction is then transported farther by the advection scheme; the repeated action of this over many time steps results in an effective, artificial transport of the particles into the upper stratosphere. The modified Walcek and the pseudo-equilibrium schemes show essentially a similar picture, although the pseudo-equilibrium scheme produces a somewhat sharper vertical gradient as it produces higher sedimentation flows above local maxima (see above and Figure 3b). Although aerosol concentrations that may be associated with numerical diffusion tend to be only marginal in comparison to the lower part of the stratosphere that is directly influenced by sulfur injection, the artificial upward transport may have an influence on the stratospheric radiation balance, and thus on circulation [e.g., Schmidt *et al.*, 2010]. Also, it has to be noted that concurrent microphysical processes, which were intentionally not considered in this study, may eventually change the picture of the relevance of low-diffusive sedimentation schemes to limit upward aerosol transport within the stratosphere. Thus, the onset of evaporation may change the vertical gradient of particle concentration, which may in turn influence vertical transport patterns.

[28] Interestingly, as shown in Table 1, the global burdens of the 100 nm-sized aerosol particles do not change much, irrespective of the occurrence of sedimentation and its formal representation. Switching on sedimentation results in a marginal decrease of the global burden by only approximately 7%. Thus, although sedimentation is very important in determining the stratospheric distribution of the aerosol particles, as seen in Figures 5a–5d, it is apparently not the dominant process in our simulations for determining the aerosol burden, and thus in turn the aerosol lifetime (Table 1, given as  $e$ -folding removal time, for definition see following section).

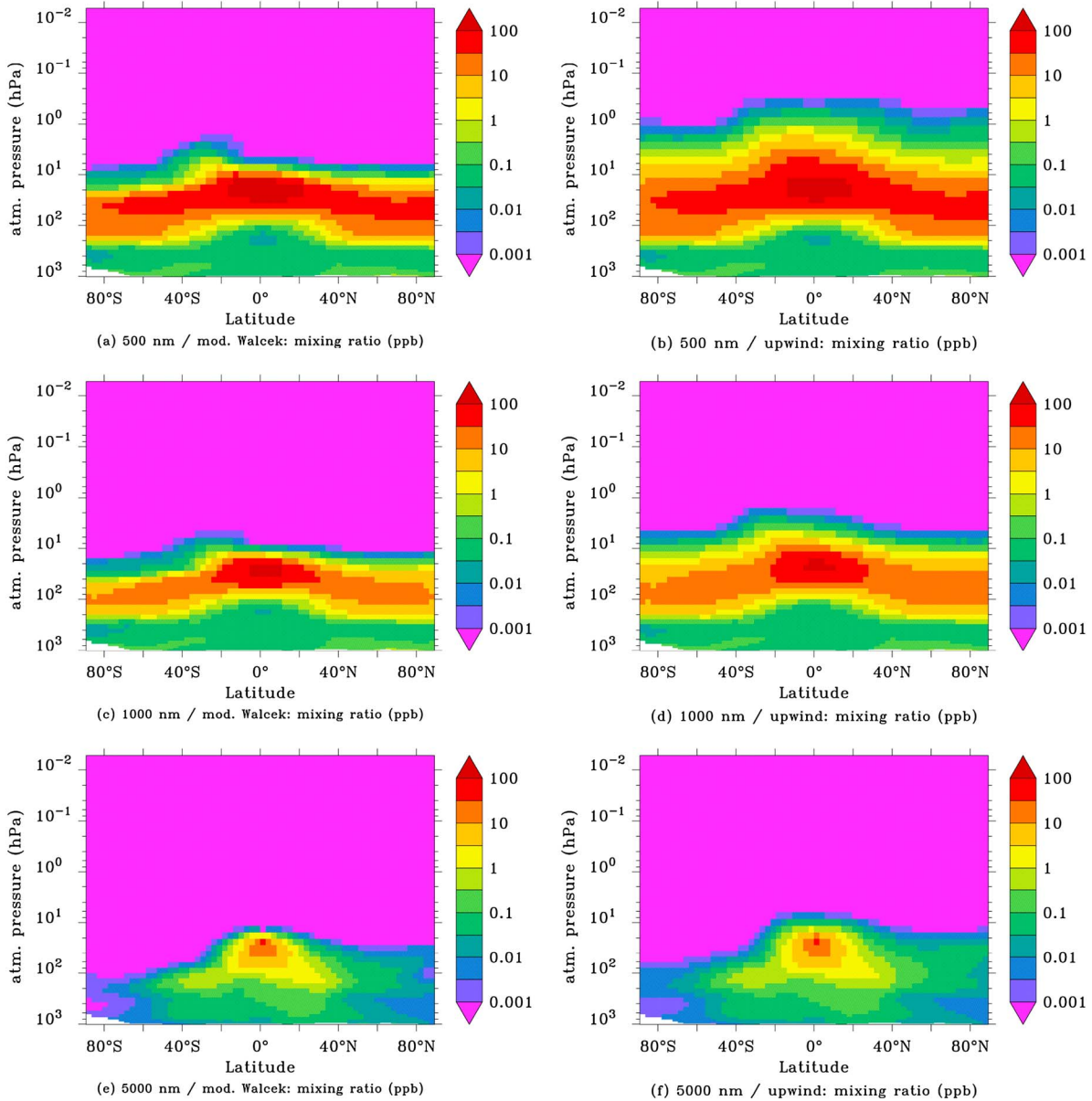


**Figure 6.** Zonal mean distribution of the S-SRM sulfate aerosol, obtained for (a, b) 500 nm, (c, d) 1  $\mu\text{m}$ , and (d, e) 5  $\mu\text{m}$  particles, with the modified Walcek and the upwind scheme, respectively. The sulfate aerosol mass distribution is given as molecular mixing ratio equivalent. See also Figure 5 for more details.

In particular, the lifetimes are nearly 3 years for all three cases with sedimentation, considerably longer than the nominal 1 year lifetime that is often assumed for sulfate particles in the unperturbed stratosphere [e.g., *Rasch et al.*, 2008a]. This is certainly related to the absence of aerosol microphysical processes, in particular evaporation, which continuously reduces the mass of particles that are moved toward the upper stratosphere, and coagulation, which tends to produce large particles that may then be removed through sedimentation (see also below). However, with passive tracers it still remains questionable whether the increase in lifetime may be exclusively imputed to the direct action of sedimentation. As noted above, when sedimentation is switched off, the aerosol distributes homogeneously within the stratosphere so that its concentration at the tropopause is somewhat

lowered, thus resulting in a lower exchange rate through both sedimentation and passive transport. As a consequence, less aerosol may be removed within the troposphere resulting in turn in a higher global burden. It is not clear whether the direct sedimentation or the feedback process via passive transport and distribution within the stratosphere is more effective in determining aerosol transport toward the troposphere. However, sedimentation as a transport process toward the troposphere is limited enough for all sedimentation schemes to show only very minor differences in the global aerosol burden.

[29] Figures 6a–6f show zonal mean plots for the generated aerosol layer with 500 nm, 1  $\mu\text{m}$ , and 5  $\mu\text{m}$  particles, obtained with the modified Walcek and the upwind scheme, respectively. When compared to the 100 nm plots, it

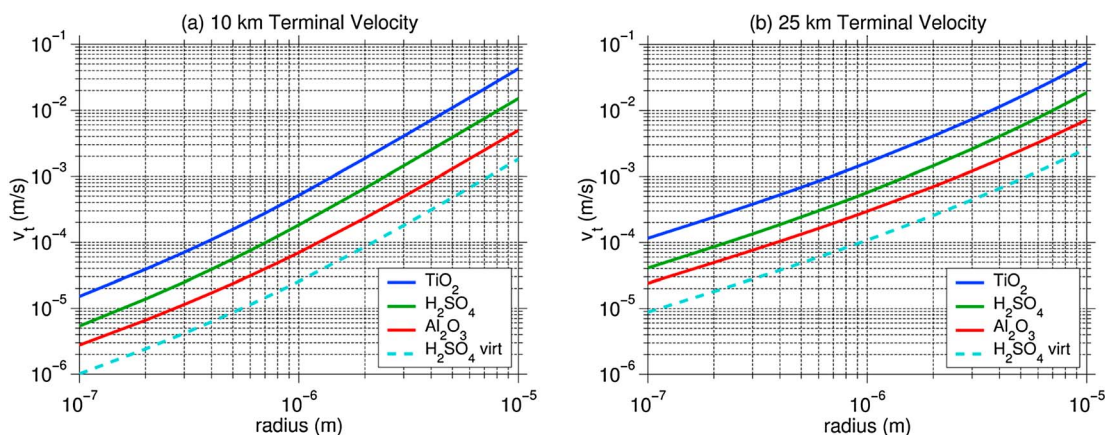


**Figure 7.** Terminal fall velocities of spherical sulfate and  $\text{TiO}_2$  particles, as opposed to cylindrical disk-shaped  $\text{Al}_2\text{O}_3$  and virtual particles of a density similar to sulfate aerosol, under atmospheric conditions typical at (a) 10 and (b) 25 km.

appears that sedimentation tends to progressively constrain particles much more effectively to the lower stratosphere with increasing terminal velocities (see Figure 7 for terminal velocities as a function of particle size at 10 and 25 km, respectively). It appears that terminal velocities show strong height dependence, mainly due to the Cunningham slip flow correction, which depends on both temperature and atmospheric pressure via the air molecule mean free path. Terminal velocities for 100 nm particles vary by 1 order of magnitude between 10 and 25 km, whereas micrometer particles sediment 3 times faster. As a result of their generally higher speed, larger particles are less susceptible to numerical diffusion, since the overestimation of covered distances is less pronounced, which results in a somewhat reduced contrast between Figures 6a, 6c, and 6e on the one hand and Figures 6b, 6d, and 6f on the other hand when compared to Figures 5a and 5c. For 5  $\mu\text{m}$  particles, the associated sedimentation losses are so pronounced that the height of maximum in the stratosphere is displaced toward the tropopause, with an apparent spillover of particles into the troposphere and a considerably reduced meridional transport efficiency in the stratosphere. Similarly, a significant spillover of 1  $\mu\text{m}$  particles into the upper troposphere may be observed underneath the injection site. If this effect were to be confirmed, it could lead to significant heating below the tropical tropopause [Heckendorn *et al.*, 2009] and/or a significant modification of cloud microphysical properties, with possible consequences to the tropical radiation balance and circulation patterns.

[30] The associated global aerosol burdens and estimated lifetimes are shown in Table 1. It is clear that especially the 1 and 5  $\mu\text{m}$  particles are considerably more affected by sedimentation than the 100 nm particles. In the 1  $\mu\text{m}$  case both the lifetime and the global burden are reduced by more than 50%, while for 5  $\mu\text{m}$  particles the global burden reduction exceeds 95%. For 500 nm particles, the reduction of the global burden amounts to some 27.5%. The differences among the tested schemes are also significantly more pronounced, with the upwind scheme resulting in an approximately 3.5% larger burden than the modified Walcek scheme with 1  $\mu\text{m}$  particles, as these move farther up into the stratosphere and removal through the tropopause is more effectively prevented. However, both the residence time and the global burden remain within the same order of magnitude as what we use

when the formation and relevance of 1  $\mu\text{m}$  particles within S-SRM scenarios is estimated (see Appendix A). It therefore appears that sedimentation is still not a substantially faster process relative to passive transport mechanisms, such that large particles may be expected to form through coagulation during the related long particle residence time. The secondary nature of the relevance of sedimentation will be confirmed in the following section.

## 7. Relationship Between Particle Properties and Sedimentation

[31] Within the previous section, we have seen that within a size range that should typically comprise both S-SRM and volcanic particles, the influence of sedimentation on stratospheric aerosol lifetime increases from insignificant, to secondary and finally dominating. The particles that we used in our simulations were assumed to be spherical and to be binary solutions of sulfuric acid and water. However, sulfur is not the only chemical species currently under consideration to undertake S-SRM, while volcanic particles also contain a certain amount of ash. Alternatively, the use of solid particles is being investigated for purposes of S-SRM, with crystal titanium dioxide ( $\text{TiO}_2$ ) and aluminum oxide ( $\text{Al}_2\text{O}_3$ ) being among the species that are considered due to their favorable radiative properties [see, e.g., Pope *et al.*, 2012], in the sense that these species reflect solar radiation more effectively than sulfate aerosol, while they are less effective absorbers of terrestrial radiation. Due to their favorable terrestrial radiation properties, massive local warming effects of the stratosphere should be less likely (were these to occur, they could in turn lead to substantial perturbations of the stratospheric circulation, with possible implications for tropospheric circulation, and a potential enhanced stratospheric ozone depletion effect).

[32] In order to investigate the relationship between the relevance of sedimentation as a lifetime limiting process, and particle size, shape, and chemical nature, we will first attempt to establish a more concise formalism for the relationship between size and sedimentation losses. Using a box concept for the stratosphere, and further, making the

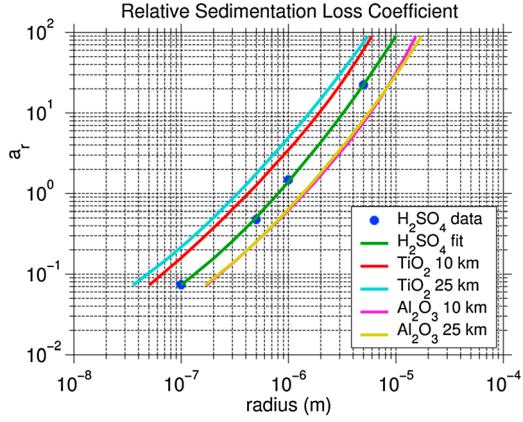


**Figure 8.** Relevance of sedimentation losses relative to passive transport losses given as a function of particle radius for sulfate aerosol, spherical  $\text{TiO}_2$  particles, and cylindrical disk-shaped  $\text{Al}_2\text{O}_3$  particles. The ratio between the cylinder radius and height is assumed to be equivalent to 10. Sulfate aerosol data points are displayed. The curves of the solid particles are assessed with a conceptual approach, based on the assumption of equal sedimentation losses at equal terminal velocities at a representative height of the tropopause, which is tentatively set to 10 km (see text).

assumption that the losses through transport and sedimentation are not interdependent and thus additive, one obtains

$$\frac{dM}{dt} = I - aM \approx I - (a_{Tr} + a_{Sed})M,$$

where  $M$  stands for the total aerosol tracer mass in the stratosphere [Mt S],  $I$  stands for the injection rate of that tracer into the stratosphere [Mt S/a], and  $a$  stands for its removal rate [ $\text{a}^{-1}$ ], which then breaks down into the removal through transport ( $a_{Tr}$ ) and sedimentation ( $a_{Sed}$ ). We have chosen non-SI units for increased readability. The  $e$ -folding removal time of tracer mass, which will be henceforth associated with the aerosol stratospheric lifetime, is given thus by  $\tau = a^{-1}$ .

[33] One may also define the relative sedimentation rate as

$$a_r = a_{Sed}/a_{Tr}.$$

[34] The solution of the preceding linear first-order differential equation is relatively straightforward; with  $M(t=0)=0$ , one obtains

$$M = \frac{I}{a}(1 - e^{-at}).$$

[35] At an infinite time scale, this equation tends to  $M(t \rightarrow \infty) \equiv M_T = I/a$ .  $a_{Sed}$  may be isolated from  $a$  under the above additivity assumption of sedimentation and transport losses provided that  $a_{Tr}$  is known. For simulations without sedimentation, one finds  $a_{Tr} = a$ , which would thus have a similar value within simulations that include sedimentation as a loss process. By the end of our simulation period, the total aerosol mass may be assumed to be sufficiently stable, such that from Table 1  $M_T \approx 30.016$  Mt S, and  $I = 10$  Mt S/a, one obtains  $a_{Tr} = 0.3332 \text{ a}^{-1}$ . For the global burden, we have chosen the value obtained with the modified Walcek sedimentation

scheme, as the most accurate one. Since the total mass dependency is quite restricted, we will not discuss removal rates as a function of the sedimentation scheme.

[36] The values of the relative sedimentation loss rate  $a_r$  may now be obtained as a function of particle size. The corresponding data points are shown in Figure 8 in combination with a fitted transient curve that has the following shape:

$$\log_{10} a_r = A + B \log_{10} r + C \log_{10}^2 r,$$

with  $A = 0.2608105507287$ ,  $B = 4.6739030261812$ , and  $C = 18.8003323345879$ , for  $r[\text{m}]$ , and  $a_r[-]$ .

[37] Within the limits of our simplifying assumptions, it appears from Figure 8 that sedimentation losses amount to less than 10% of passive transport losses through the tropopause and may thus be called negligible, for  $r < 120$  nm. Above this size, the influence of sedimentation increases rapidly to reach about an equal amount of sedimentation and transport losses at about  $r = 800$  nm. For particles larger than 3  $\mu\text{m}$ , sedimentation losses are more than 10 times more relevant than transport losses.

[38] The assumption that transport and sedimentation may be separated could potentially distort the picture we obtained with respect to the relative influence of sedimentation losses. Within this study we have chosen an injection height of 25 km. Since there are no evaporation effects included, the injection height should not affect the values of  $a_r$  we have obtained, unless there is height-dependent interaction between the processes of passive transport and sedimentation. We alluded to this circumstance in the previous section already and cannot assess its relevance here in the absence of relevant data. For this reason the figures obtained here need to be treated with due caution and primarily serve as an indication for the distinction of the respective removal regimes.

[39] Let us now investigate the role of the particle chemical nature, which primarily influences the sedimentation properties via particle density and their shape. As mentioned above, materials currently under discussion include  $\text{TiO}_2$  and  $\text{Al}_2\text{O}_3$ .  $\text{TiO}_2$  may be produced as a powder [e.g., *Jang and Kim, 2001*], whose individual aggregated nanoparticles may be associated with spheres in terms of their hydrodynamic free fall properties [*Pruppacher and Klett, 1997*, p. 452], while  $\text{Al}_2\text{O}_3$  may be produced both as nanospheres and irregular nanoplatelets [*Pang and Bao, 2002*]. In order to investigate the influence of particle size on the sedimentation behavior, we chose  $\text{Al}_2\text{O}_3$  particles to be nanoplatelets, which we associate with the shape of cylindrical disks.

[40] In the absence of corresponding model simulations with solid particles, the significance of sedimentation as a function of particle size has to be assessed with indirect means using the available data for sulfate particles. Here we use the ansatz of establishing the analogy via the terminal fall velocity. This procedure, although somewhat ad hoc, makes sense if we consider that the sedimentation loss rate  $a_{Sed}$  in our above 0-D box approach actually corresponds to the net sedimentation driven downward flux of particles through the tropopause in a 3-D model environment. The dimensionality of the 3-D model flux would thus be represented by the length scale present in the terminal velocity as opposed to  $a_{Sed}$ , which is exclusively expressed in terms of a timescale.

[41] Figure 7 compares the terminal velocity of sulfur and  $\text{TiO}_2$  spheres as opposed to cylindrical  $\text{Al}_2\text{O}_3$  disks, at a

**Table 2.** Aerosol Global Burden and Lifetime as a Function of Chemical Composition<sup>a</sup>

	Sulfur		Titanium Dioxide <sup>b</sup>		Aluminum Oxide <sup>b</sup>	
	Burden (%)	Lifetime (years)	Burden (%)	Lifetime (years)	Burden (%)	Lifetime (years)
100 nm	93.18%	2.7968	<i>86.27%</i>	<i>2.5894</i>	<i>95.14%</i>	<i>2.8557</i>
500 nm	67.59%	2.0288	<i>44.29%</i>	<i>1.3295</i>	<i>80.51%</i>	<i>2.4165</i>
1000 nm	40.41%	1.2128	<i>21.79%</i>	<i>0.6540</i>	<i>62.63%</i>	<i>1.8800</i>
5000 nm	4.29%	0.1286	<i>1.66%</i>	<i>0.0499</i>	<i>10.76%</i>	<i>0.3230</i>

<sup>a</sup>See text for corresponding densities and shapes.

<sup>b</sup>Values in italics are deduced from the respective terminal velocities. Obtained with the modified Walcek scheme. See Table 1 for additional explanations.

height of 10 and 25 km, respectively. Results are also given for virtual cylindrical particles of a density  $\rho = 1.5 \text{ g/cm}^3$ , which also stands for the typical density of binary sulfuric acid and water solutions. The density of crystal  $\text{TiO}_2$  is  $\rho = 4.23 \text{ g/cm}^3$ , while the density assumed for  $\text{Al}_2\text{O}_3$  is  $\rho = 4.10 \text{ g/cm}^3$  (for densities, see, e.g., *Lide* [2003]). Due to the size of the particles considered here, and their associated Reynolds number, the fall velocity of both spherical and cylindrical particles may be approximated to be in the Stokes regime, while the air dynamic viscosity has to be corrected for the Cunningham slip flow [see *Pruppacher and Klett*, 1997, p. 416f.]. For disk-shaped nanoparticles, the Stokes regime terminal fall velocity has to be corrected for drag, volume, and slip flow, taking into account the variability of the orientation of the particles during their fall. Following *Dahneke* [1973a, 1973b] for the drag and slip flow correction, and assuming a cylinder radius to height ratio of 10, we find the following relationship for the terminal velocity  $v_T$  of cylindrical disks:

$$v_{T,CD} = \frac{\pi r_{CD}^2 (\rho_p - \rho_a) g}{120\mu_a} C_{CD},$$

where  $r$  stands for the cylinder radius,  $\rho$  is the density,  $g$  is the gravity acceleration,  $\mu$  is the dynamic viscosity, and  $C$  is the Cunningham slip flow correction factor. The indices  $CD$ ,  $p$ , and  $a$  stand for “cylindrical disk,” “particle,” and “air,” respectively. The Cunningham factor is obtained for cylindrical disks using the adapted radius  $r_a$  in the assessment of the Knudsen number. For cylindrical disks of negligible height,  $r_a = 0.522 r_{CD}$ .

[42] As shown in Figure 7, the terminal velocity of  $\text{TiO}_2$  particles is highest due to their higher density. Due to their aerodynamic properties, and their lower volume to surface ratio, the terminal velocity of  $\text{Al}_2\text{O}_3$  disks would be substantially lower. The near-linear relationship (with the exception of the slip flow correction) of the terminal velocities of spherical and disk-shaped particles in the Stokes regime is depicted by the apparent parallel nature of the results.

[43] We will now try to produce predictions as to how the relationship between the relative sedimentation loss factor  $a_r$  and particle radius would be like for  $\text{TiO}_2$  and  $\text{Al}_2\text{O}_3$  particles. In the absence of corresponding model results, the resulting relationship should only be considered as a plausible illustration of the actual relationship, in particular with respect to the simplifications that go into the formulation of  $a_r$ , and the approximate character of our assumptions that lead to the analogy between  $a_r$  and the terminal velocity.

[44] Based on the assumed principle that for similar terminal velocities, similar relative sedimentation loss factors would be found, the relationship between  $a_r$  and the radius of  $\text{TiO}_2$  and

$\text{Al}_2\text{O}_3$  particles may be established following the following chain of functions:

$$a_{r,\text{TiO}_2} \equiv a_{r,\text{sulf}} \rightarrow r_{\text{sulf}} \rightarrow v_{T,\text{sulf}} \equiv v_{T,\text{TiO}_2} \rightarrow r_{T,\text{TiO}_2}.$$

[45] The inherent uncertainty of the relationship resides in the choice of a representative relevant height at which the terminal velocities are equalized, which would stand for a process averaged height of the tropopause (see above). This height has been tentatively set to 10 km.

[46] In order to relate particle radius to their terminal velocities, parameterizations of the following shape have been established:

$$\log_{10} v_T = \sum_{i=0}^2 A_i \log_{10}^i r.$$

[47] The resulting relationship between the size of  $\text{TiO}_2$  and  $\text{Al}_2\text{O}_3$  particles and their relative sedimentation loss rate is depicted in Figure 8. For the illustration of the relevance of the representative tropopause height, the relationship that would be obtained with a value of 25 km is depicted as well. The dependence of the deduced size/sedimentation loss rate functions on the representative tropopause height is relatively low. For the more plausible 10 km case,  $\text{TiO}_2$  particles would experience tenfold domination of passive transport losses at a size of 70 nm, similar sedimentation and transport losses would occur at approximately 400 nm, and a tenfold domination of sedimentation losses would take place at about  $r = 2 \mu\text{m}$ . Comparable sedimentation loss rates of  $\text{Al}_2\text{O}_3$  disks would occur at significantly larger sizes. Passive transport losses would be tenfold more efficient at 200 nm, sedimentation and transport losses would be similar at about  $1.5 \mu\text{m}$ , and tenfold domination of sedimentation losses would occur at  $8 \mu\text{m}$ . The related global burdens and e-folding lifetimes for  $\text{TiO}_2$  and  $\text{Al}_2\text{O}_3$  particles are summarized in Table 2 and compared against the sulfate particle data obtained with global model experiments with the modified Walcek scheme.

[48] In summary, with respect to the optimal surface/volume ratio in terms of the particle radiative properties (see above) and the derived optimal S-SRM particle size of the order of 100 nm, solid spherical particles would experience significant, however, still minor sedimentation losses due to their comparatively higher density, provided that they do not experience significant aggregation. Disk-shaped particles of comparable size would experience negligible sedimentation losses throughout a large fraction of the considered size range, such that potential particle aggregation would not lead to substantial losses either. Sedimentation would be

the dominating removal process of liquid spherical particles for  $r > 800$  nm, which may be obtained under conditions of S-SRM depending on their actual lifetime and growth dynamics. Conversely, high-density solid spherical particles used for S-SRM would under no circumstance reach a size at which they could become relevant in terms of terrestrial radiation, as they would be removed by sedimentation prior to reaching this size. In terms of sedimentation losses, disk-shaped particles could be released at a comparably large size. However, it should be noted that from mass considerations, such particles would tend not to make sense, due to the relatively high mass injection rates that would be required to achieve the desired radiative effect. With respect to volcanic ash particles, which may most realistically be associated with spherical  $\text{TiO}_2$  in terms of their shape and density, our findings underline the relative importance of sedimentation for these particles, and the tendency for these particles to show relatively low residence times in the stratosphere.

## 8. Discussion and Conclusion

[49] Using newly developed sedimentation schemes, the present paper explores the role sedimentation plays as a limiting factor for the lifetime of stratospheric aerosol with a special focus on particles that would likely be used in the context of stratospheric solar radiation management (S-SRM).

[50] Validation tests have shown that apart from their low-numerical diffusion property, these schemes should produce particularly good results in the context of conservation of pronounced maxima, such that they should be particularly suitable for the simulation of S-SRM scenarios.

[51] The analysis of size sensitivity tests with an aerosol chemistry general circulation model has shown that for the shapes and densities considered, sedimentation plays a secondary role for the lifetime of particles within a size range that is considered to be optimal for S-SRM purposes. On the other hand, aerosol lifetime has been shown to be dominated by sedimentation once a substantial fraction of the aerosol particles would either grow beyond a certain size through microphysical processes or be emitted at that size. The latter circumstance would especially apply for high-density spherical particles, such as mineral dust emitted in the context of volcanic eruptions or  $\text{TiO}_2$  nanoparticles, while such a scenario would be relatively unlikely for disk-shaped particles due to their aerodynamic properties and surface/volume ratio. Estimated sedimentation loss rates as a function of particle size and growth dynamical considerations have led us to the conclusion that liquid sulfate particles may reach a size at which sedimentation would become a substantial removal process.

[52] For this reason it is of primary importance to accurately represent the processes, namely troposphere-stratosphere exchange and sedimentation, which in association with aerosol microphysics (in particular coagulation and evaporation for liquid and aggregation for solid particles) determine the aerosol lifetime in the stratosphere. To that effect, the microphysical scheme used in the model environment needs to have limited numerical diffusion properties, or when a modal scheme (rather than a bin scheme) is used, special care needs to be taken in order for intermodal exchange to be accurately represented.

[53] Although the bulk number of secondary particles does not normally grow beyond micrometer size on a time scale typically associated with the Brewer-Dobson circulation, still a significant mass fraction might eventually tend to concentrate within particles exceeding this size. Therefore, the relationship between the global injection strategy, mean particle size, and the aerosol mean age merits extensive investigation.

[54] With respect to stratosphere troposphere exchange, it appears that the relevance of numerical diffusion in the adopted sedimentation scheme is only marginal. However, the usage of a scheme that minimizes numerical diffusion was shown to be particularly relevant to prevent artificial upward transport of smaller aerosol particles to the middle or upper stratosphere, with possible consequences for an accurate simulation of ozone depletion and stratospheric circulation modification patterns in the context of either S-SRM or volcanic eruptions.

[55] As a conclusion, this study allowed identifying the main characteristics of sedimentation in the context of a stratosphere subjected to S-SRM. It found that (1) the numerical diffusion associated with sedimentation schemes may lead to undesirable transport of the aerosol to the upper stratosphere and that (2) in the context of S-SRM, the actual relevance of sedimentation is subject to a multitude of aerosol properties, mainly size, shape, density, and microphysical growth properties. Apart from being a function of S-SRM scenarios, the quantification of the actual relevance of sedimentation as a limiting factor of the efficiency of S-SRM therefore requires a very accurate representation of the interaction of aerosol growth dynamics, atmospheric circulation and sedimentation. This will be pursued in a follow-on study that will focus especially on a realistic representation of particle growth dynamics.

## Appendix A: Consideration of the Formation of Large Aerosol Particles

[56] Based on the terminal velocity function of aerosol particles in the Stokes regime, significant sedimentation losses of stratospheric aerosol may be associated with particles exceeding  $r = 1$   $\mu\text{m}$ . However, it is not clear whether coagulation of liquid secondary particles will lead to the formation of a significant amount of 1  $\mu\text{m}$  and even larger particles in the context of S-SRM. Although particles of 1  $\mu\text{m}$  radius and larger have been observed in the context of volcanic eruptions [Russell *et al.*, 1996], prescribed accordingly within model simulations in the same context [Timmreck *et al.*, 2010], and modeled in the context of S-SRM [Heckendorn *et al.*, 2009], it has to be noted that the formation process of large volcanic particles is dissimilar to proposed S-SRM. Thus, the formation of large particles is effectively enhanced by the presence of preformed primary particles, whereas aerosol growth may be too slow under dominantly secondary conditions for such particles to appear even on very long timescales typical to the stratosphere. A related concern is the relationship between the formalism of modal aerosol growth models and the formation of coarse mode particles. Sectional Eulerian aerosol microphysics models, and in particular modal models, used in the context of global modeling, are known to be potentially very diffusive across size sections [Korhonen *et al.*, 2003] and therefore less suitable for aerosol growth simulation under the

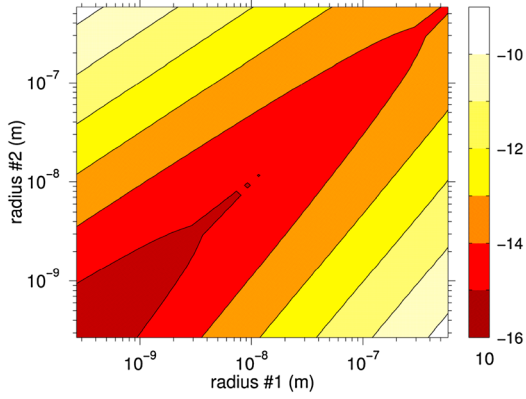


**Figure A1.** Brownian coagulation kernel ( $\text{m}^3 \text{s}^{-1}$ , on logarithmic scale) at 25 km (1976 Standard Atmosphere) as a function of the size of the colliding particles. Due to the relatively high mean free path of particles at the low air density of 25 km, coagulation essentially takes place in the molecular regime, even for micrometer-sized particles. Calculations are made according to *Fuchs* [1964].

long timescale conditions associated with the stratosphere. Less diffusive, hybrid Eulerian-Lagrangian models have been developed for use within 3-D models [*Zhang et al.*, 1999]. These models only reduce numerical diffusion in relationship with the process of condensation; they do not take into account numerical diffusion via coagulation. Diffusive models remain largely in use (especially modal models tend to be very diffusive due to their coarse size resolution), and little focus was given so far to this question in the context of S-SRM. It may therefore be possible that the large particle formation is grossly overestimated within global simulations as a result of numerical diffusion.

[57] The unlikelihood of the formation of a large number of particles larger than  $1 \mu\text{m}$  may be illustrated with simple mass balance and growth dynamical considerations. If we assume a 10 km deep homogeneous aerosol layer in the stratosphere, the artificial aerosol would fill a volume of approximately  $5 \cdot 10^{18} \text{m}^3$  on the global scale. If the total mass of the particles was equivalent to 10 Mt S and the particles had a volume mean size of  $1 \mu\text{m}$ , their total number would be of the order of  $10^{25}$ , thus resulting in an equivalent number density of the order of only  $1 \text{cm}^{-3}$ . The order of magnitude of the time interval that would be required for particles to reach micrometer size may be estimated under the assumption that neither condensation nor dilution contributes significantly to the growth behavior of the aerosol particles, so that coagulation would be the only relevant growth process. Dilution and condensation may actually be neglected as these should only contribute to aerosol growth during the initial period following the release of sulfur into the stratosphere, upon which particles should still be relatively small [*Turco and Yu*, 1997]. The accuracy of this assumption will be shown below. The Brownian coagulation kernel [*Fuchs*, 1964], as depicted in Figure A1, is a strong function of particle size. At a height of 25 km, coagulation essentially takes place in the molecular regime up to micrometer size due to the relatively large mean free path of the aerosol particles in the dilute air medium. At sea level, coagulation takes place in the transition regime when the larger particle is more than

about  $r = 0.1 \mu\text{m}$  large (not shown). Particles of dissimilar size tend to collide much more frequently than particles of similar size. This results in a narrowing of the aerosol spectrum as relatively small particles are preferentially removed, whereas the probability of obtaining large particles is relatively small, as these require a much larger number of coagulation events. S-SRM particles are likely to develop the resulting self-preserving size distribution [*Friedlander and Wang*, 1966; *Lai et al.*, 1972], as the associated residence times are high and mixing processes are relatively slow. Aerosol particles have been shown to develop a self-preserving distribution, regardless of whether their evolution is governed purely by coagulation or whether condensation and nucleation also take place simultaneously [*Pratsinis*, 1988].

[58] The estimation of aerosol growth time may be further simplified by the fact that we force the aerosol particles to remain monodisperse during the growth by coagulation. This allows us to associate the entire time interval with a certain amount of discrete time intervals, each standing for the amount of time required by the monodisperse aerosol to double its size. Furthermore, the particle growth velocity may be assumed to be constant during each discrete time interval. However, we need to explore to what extent the average coagulation kernel of a self-preserving aerosol differs from the monodisperse kernel. When the self-preserving aerosol is assumed to be lognormally distributed with logarithmic standard deviation, typically  $\sigma = 0.5$  [*Lee et al.*, 1984; *Pratsinis*, 1988], then the relationship between the monodisperse coagulation kernel and the average coagulation is as follows for the diffusion regime case:

$$\begin{aligned} & \frac{0.5a}{0.5k_{m,d}N^2} \int_0^\infty \frac{\partial N}{\partial R} dR \int_0^\infty (r+R)(r^{-1}+R^{-1}) \frac{\partial N}{\partial r} dr \\ &= \frac{2aN^2 + 2a\langle r \rangle \langle r^{-1} \rangle N^2}{k_{m,d}N^2} = 0.5(1 + e^\sigma) \approx 1.3, \end{aligned}$$

with  $k_{m,d} = 4a$  being the monodisperse coagulation kernel  $k_m$  in the diffusion regime.

[59] In the molecular regime, the corresponding equation is

$$\begin{aligned} & \frac{0.5a}{0.5k_{m,m}N^2} \int_0^\infty \frac{\partial N}{\partial R} dR \int_0^\infty (r^2+R^2)(r^{-3}+R^{-3})^{0.5} \frac{\partial N}{\partial r} dr \\ & < \frac{2\sqrt{2} \cdot a \langle r^2 \rangle \langle r^{-3/2} \rangle N^2}{k_{m,m}N^2} = e^{2.375\sigma} \approx 3.3, \end{aligned}$$

with  $k_{m,m} = 2\sqrt{2}ar_m^{0.5} = 2\sqrt{2}a\langle r^3 \rangle^{1/6}$  being the monodisperse coagulation kernel in the molecular regime.

[60] The above equations were obtained considering the moments  $\langle r^n \rangle = e^{n\mu + 0.5n^2\sigma}$  of the lognormal distribution function. They show that in whatever regime coagulation is, the mean coagulation kernel of a lognormally distributed aerosol is of the same order of magnitude as the corresponding monodisperse kernel.

[61] If we consider that a  $1 \mu\text{m}$  particle contains of the order of  $10^{10}$  sulfuric acid molecules, then each particle must have undergone approximately 35 monodisperse growth steps prior to reaching this size, each growth step resulting in a halving of the number of particles and a doubling of the number of molecules per particle. Then, the discretely

backward integrated estimated time interval for growth to micrometer size becomes

$$\Delta t = \sum_{i=1}^{35} dt_i \cdot n_i = \sum_{i=1}^{35} (0.5 \cdot \langle k \rangle_i \cdot 2^{2i} n_0^2)^{-1} \cdot 2^{i-1} n_0 \approx \langle k \rangle^{-1} n_0^{-1} \sum_{i=1}^{35} 2^{-i} \approx \langle k \rangle^{-1} n_0^{-1},$$

with  $dt$  being the unit volume coagulation period [ $\text{m}^3\text{s}$ ],  $\langle k \rangle \approx k_m \approx 10^{-15} - 10^{-14} \text{ m}^3\text{s}^{-1}$  being the effective coagulation kernel,  $n_i$  being the particle number concentration during the  $i$ th backward coagulation increment [ $\text{m}^{-3}$ ], and  $n_0 = 10^6 \text{ m}^{-3}$  being the eventual  $1 \mu\text{m}$  particle number concentration.

[62] The effective coagulation kernel  $\langle k \rangle$  is averaged for the discrete size distribution within the self-preserving mode and associated according to the above equations with the corresponding monodisperse kernel  $k_m$ , which spans through the given interval of orders of magnitude as particles grow from molecular to micrometer size. It should be noted that the above equation is independent of the initial particle number concentration and thereby in accordance with Friedlander's self-similarity ansatz [Friedlander and Wang, 1966]. Also, it reflects that the bulk of the total growth time may be associated with the later stages when the aerosol concentration is relatively low, as a moderate reduction in the number of growth steps does not significantly change the total growth time. For this reason our initial assumption of neglecting dilution and condensation is proven to be accurate.

[63] According to the preceding equation,  $\Delta t$  should be of the order of 3 to 30 years for a final particle number concentration of the order of  $1 \text{ cm}^{-3}$ , and it seems therefore unlikely that the bulk of the aerosol would be able to reach micrometer size in an S-SRM scenario. The action of sedimentation, which as a competing removal process may effectively reduce the formation of large aerosol particles, should further reduce the quantity of large S-SRM aerosol particles. However, it may nevertheless be possible for a sufficient fraction of the aerosol mass to reach micrometer sizes to be relevant for S-SRM scenarios, which thus deserves further consideration. In this sense, the previous equation may also be used to assess the average size of particles if an average lifetime of 1 year is assumed and sedimentation is neglected, thereby opening the perspective to assess the fraction of aerosol mass contained in particles larger than a certain size. For an average coagulation kernel of  $\langle k \rangle = 10^{-15} - 10^{-14} \text{ m}^3\text{s}^{-1}$  and a global aerosol burden of  $10 \text{ Mt S}$  homogeneously distributed within a volume of  $5 \cdot 10^{18} \text{ m}^3$  (see above), the corresponding average particle size should be of the order of  $\langle r^3 \rangle^{1/3} = 200 - 500 \text{ nm}$ . If self-preserving particles are assumed to be lognormally distributed with logarithmic standard deviation typically  $\sigma = 0.5$  (see above), then one finds solving  $\langle r^n \rangle^{1/n} = e^{\mu + 0.5n\sigma}$  for the logarithmic average size  $\mu = -16.2$  and  $\mu = -15.2$ , with  $n = 3$ . The mass fraction contained in particles larger than  $1 \mu\text{m}$  in size should therefore be equivalent to

$$0.5 \operatorname{erfc}\left(-\frac{\ln x - \mu}{n\sigma\sqrt{2}}\right) = 0.5 \operatorname{erfc}\left(\frac{\mu + 13.81}{1.5\sqrt{2}}\right) = 0.05 - 0.175,$$

$\operatorname{erfc}$  being the complementary error function.

[64] Considering the approximate character of these estimations, it cannot be excluded that a relevant fraction of the aerosol mass in a S-SRM framework may reach micrometer size and above, depending on the average lifetime and the injection rate of sulfur.

[65] **Acknowledgments.** The present study was done within the EU 7th Framework project IMPLICC on Implications and risks of engineering solar radiation to limit climate change (implicc.zmaw.de) and was partly supported by the Institute for Advanced Sustainability Studies, funded through the German Ministry for Education and Research (BMBF) and the Brandenburg state Ministry for Science, Research and Culture (MWFK). The authors wish to thank their project partners for their support. The authors would also like to thank the reviewers for their constructive criticism, which has substantially helped improve this paper.

## References

- Bala, G., P. B. Duffy, and K. E. Taylor (2008), Impact of geoengineering schemes on the global hydrological cycle, *Proc. Natl. Acad. Sci.*, *105*(22), 7,664–7,669.
- Crutzen, P. J. (2006), Albedo enhancement by stratospheric sulfur injections: A contribution to resolve a policy dilemma, *Clim. Change*, *77*, 211–219.
- Dahneke, B. E. (1973a), Slip correction factors for nonspherical bodies—I. Introduction and continuum flow, *J. Aerosol Sci.*, *4*, 139–145.
- Dahneke, B. E. (1973b), Slip correction factors for nonspherical bodies—III. The form of the general law, *J. Aerosol Sci.*, *4*, 163–170.
- English, J. M., O. B. Toon, and M. J. Mills (2012), Microphysical simulations of sulfur burdens from stratospheric sulfur geoengineering, *Atmos. Chem. Phys.*, *12*, 4,775–4,793, doi:10.5194/acp-12-4775-2012.
- Friedlander, S. K., and C. S. Wang (1966), The self-preserving particle size distribution for coagulation by Brownian motion, *J. Colloid Interface Sci.*, *22*, 126–132.
- Fuchs, N. A. (1964), *The Mechanics of Aerosol*, Pergamon Press, London, UK.
- Heckendorn, P., et al. (2009), The impact of geoengineering aerosols on stratospheric temperature and ozone, *Environ. Res. Lett.*, *4*, 045,108, doi:10.1088/1748-9326/4/4/045108.
- Hobbs, P. V. (Ed) (1993), *Aerosol-Cloud-Climate Interactions*, International Geophysics Series, vol. 56, Academic Press, San Diego, California.
- Jacobson, M. Z. (1999), *Fundamentals of Atmospheric Modeling*, Cambridge University Press, Cambridge, UK.
- Jang, H. D., and S.-K. Kim (2001), Controlled synthesis of titanium dioxide nanoparticles in a modified diffusion flame reactor, *Mat. Res. Bull.*, *36*, 627–637.
- Joeckel, P., et al. (2006), The atmospheric chemistry general circulation model ECHAM5/MESSy1: Consistent simulation of ozone from surface to the mesosphere, *Atmos. Chem. Phys.*, *6*, 5,067–5,104.
- Kerkweg, A., et al. (2006), Technical Note: An implementation of the dry removal processes DRY DEPosition and SEDimentation in the Modular Earth Submodel System (MESSy), *Atmos. Chem. Phys.*, *6*, 4,617–4,632.
- Korhonen, H., et al. (2003), Simulation of atmospheric nucleation mode: A comparison of nucleation models and size distribution representations, *J. Geophys. Res.*, *108*(D15), 4471, doi:10.1029/2002JD003305.
- Lacis, A., J. Hansen, and M. Sato (1992), Climate forcing by stratospheric aerosols, *Geophys. Res. Lett.*, *19*(15), 1,607–1,610.
- Lai, F. S., et al. (1972), The self-preserving particle size distribution for Brownian coagulation in the free-molecule regime, *J. Colloid Interface Sci.*, *39*(2), 395–405.
- Lee, K. W., J. Chen, and J. A. Gieseke (1984), Log-normally preserving size distribution for Brownian coagulation in the free-molecule regime, *Aerosol. Sci. Tech.*, *3*(1), 53–62.
- Lide, D. R. (2003), *CRC Handbook of Chemistry and Physics*, CRC Press, Boca Raton, Florida, 84th edition.
- Pang, Y.-X., and X. Bao (2002), Aluminium oxide nanoparticles prepared by water-in-oil microemulsions, *J. Mater. Chem.*, *12*, 3,699–3,704.
- Pierce, J. R., et al. (2010), Efficient formation of stratospheric aerosol for climate engineering by emission of condensable vapor from aircraft, *Geophys. Res. Lett.*, *37*, L18805, doi:10.1029/2010GL043975.
- Pope, F. D., et al. (2012), Stratospheric aerosol particles and solar-radiation management, *Nat. Clim. Change*, *2*, 713–719, doi:10.1038/nclimate1528.
- Prather, M. J. (1986), Numerical advection by conservation of second-order moments, *J. Geophys. Res.*, *91*(D6), 6,671–6,681.
- Pratsinis, S. E. (1988), Simultaneous nucleation, condensation, and coagulation in aerosol reactors, *J. Colloid. Interface Sci.*, *124*(2), 416–427.
- Pruppacher, H. R., and J. D. Klett (1997), *Microphysics of Clouds and Precipitation*, Atmospheric and Oceanographic Sciences Library Kluwer Academic Publishers, Dordrecht, The Netherlands, vol. 18.
- Rasch, P. J., P. J. Crutzen, and D. B. Coleman (2008a), Exploring the geoengineering of climate using stratospheric sulfate aerosols: The role of particle size, *Geophys. Res. Lett.*, *35*, L02809, doi:10.1029/2007GL032179.
- Rasch, P. J., et al. (2008b), An overview of geoengineering of climate using stratospheric sulfate aerosols, *Phil. Trans. Roy. Soc. A*, *366*, 4,007–4,037.
- Robock, A., et al. (2013), Studying geoengineering with natural and anthropogenic analogs, *Clim. Change*, doi:10.1007/s10584-013-0777-5.

- Russell, P. B., et al. (1996), Global to microscale evolution of the Pinatubo volcanic aerosol derived from diverse measurements and analyses, *J. Geophys. Res.*, *101*(D13), 18,745–18,763.
- Schmidt, H., G. P. Brasseur, and M. A. Giorgetta (2010), Solar cycle signal in a general circulation and chemistry model with internally generated quasi-biennial circulation, *J. Geophys. Res.*, *115*, D00I14, doi:10.1029/2009JD012542.
- Seinfeld, J. H., and S. N. Pandis (1998), *Atmospheric Chemistry and Physics: From Air Pollution to Climate Change*, John Wiley & Sons, New York.
- Stenchikov, G. L., et al. (1998), Radiative forcing from the 1991 Mount Pinatubo volcanic eruption, *J. Geophys. Res.*, *103*(D12), 13,837–13,857.
- Tilmes, S., et al. (2009), Impact of geoengineered aerosols on the troposphere and stratosphere, *J. Geophys. Res.*, *114*, D12305, doi:10.1029/2008JD011420.
- Timmreck, C., et al. (2010), Aerosol size confines climate response to volcanic super-eruptions, *Geophys. Res. Lett.*, *37*, L24705, doi:10.1029/2010GL045464.
- Turco, R. P., and F. Yu (1997), Aerosol invariance in expanding coagulating plumes, *Geophys. Res. Lett.*, *24*(10), 1,223–1,226.
- Vaughan, N. E., and T. M. Lenton (2011), A review of climate geoengineering proposals, *Clim. Change*, *109*, 745–790, doi:10.1007/s10584-011-0027-7.
- Walcek, C. J. (2000), Minor flux adjustment near mixing ratio extremes for simplified yet highly accurate monotonic calculation of tracer advection, *J. Geophys. Res.*, *105*(D7), 9,335–9,348.
- Zhang, Y., et al. (1999), Simulation of aerosol dynamics: A comparative review of algorithms used in air quality models, *Aerosol. Sci. Tech.*, *31*(6), 487–514, doi:10.1080/027868299304039.